Bioaerosols standoff detection simultaneously refereed with particle concentration (ppl) and viability units (ACPLA)

Sylvie Buteau*[a], Jean-Robert Simard[a], Susan Rowsell[b]
[a] Defence R&D Canada – Valcartier, 2459 boul. Pie-XI Nord, Québec, Québec, G3J 1X5
[b] Defence R&D Canada – Suffield, PO Box 4000, Station Main, Medicine Hat, Alberta, T1A 8K6

ABSTRACT

Defence R&D Canada (DRDC) has developed, by the end of the 90s, a standoff bioaerosol sensor prototype based on intensified range-gated spectrometric detection of Laser Induced Fluorescence (LIF) called SINBAHD. This LIDAR system was used to characterize spectrally the LIF of bioaerosol agent simulants and obscurants during 57 cross-wind open-air releases at Suffield, CAN in July 2007. An autoclave and gamma-irradiation killing procedures were performed on *Bacillus subtilis var globigii* (BG) samples before they were aerosolized, disseminated and spectrally characterized. Slight discrepancies were observed in the spectral characteristics of killed versus live samples but none between the two killing methodologies. Significant signature variabilities were observed from the different batches of *Erwinia Herbicolas* (EH). The generated cloud was simultaneously characterized in Agent Containing Particle per Liter of Air (ACPLA) by slit sampler units and in particle per litter of air (ppl) by an Aerodynamic Particle Sizer (APS). Correlation assessment between the stand-off sensor SINBAHD and the two referee point sensors was done, allowing an estimation of SINBAHD's sensitivity in ACPLA and in ppl. For a 20-m thick cloud at a range of 990 m, a detection limit of a few tens of ACPLA and a few ACPLA were obtained for BG and EH respectively. The extracted correlation between ACPLA and ppl data for releases performed with an agricultural sprayer showed a high degree of variability: 2 to 29% and 1 to 6% of ACPLA/ppl ratio for BG and EH, respectively.

Keywords: Bioaerosol simulants, standoff detection, Laser-Induced Fluorescence, LIF, range-gating, ppl, ACPLA.

1. INTRODUCTION

During the last two decades, biological threats have become a growing concern for both military and civilian communities. Indeed, the rising availability of bio-warfare materials [1] and the considerable lethality of biological agents have led to an increasing biological threat. This threat can take different forms, such as air, water or food contamination, and can arise in different scenarios, such as indoor releases in a building or outdoor releases over an extended area. Different types of detection systems were and are still being developed in preparation for these various emerging threats. Detection systems currently in use [2] have the ability to detect, and in some cases identify, biological agents in time to provide treatment. However in future systems, increased emphasis will be placed on the ability to **provide early warning** of the presence of a biological threat. A given sensor performance will vary depending on the scenario in which it is employed, hence the importance of selecting a biological detector based upon the most probable scenario. Point detectors are able to detect biological threats but need to be located within the threatening cloud; they are hence not well suited for wide area monitoring.

Once illuminated by light, all aerosol particles in the atmosphere both absorb and scatter the incoming light energy. All particles will scatter light, but absorption can occur only at specific wavelengths where allowed electronic transitions specific to the aerosol matter exist. Scattering from a molecule is called Rayleigh scattering, while Mie scattering is from aerosols. Hence, illuminating a biological aerosol cloud with a laser pulse will produce Mie scattering, with a portion of the energy being backscattered to the laser receiver. This technique is called elastic backscatter lidar. The amplitude of the return signal is proportional to the number of aerosolized particles present in the probed volume, while the time delay of the return signal is related to the distance from the cloud. Elastic backscatter lidar systems, typically operating in the infrared range (1 to 10 μm) can detect aerosol clouds up to a few tens of kilometers away [3]. Inelastic lidar can procure specific information on the light scattering particles following the absorption and emission of a photon at different frequencies either through a virtual energy level, in the case of Raman lidars, or through a real excited state for the resonant lidars. The former is characterized by a spectrally narrow return signal presenting a shift in light frequency

independent of the irradiation wavelength. The return signal of the resonant lidar, which is called laser-induced fluorescence (LIF), can either be spectrally narrow or distributed over a wide spectral interval, depending on the complexity of the atomic structure of the excited aerosol [4]. Since this technique involves a resonant effect, the irradiating wavelength is critical and must be chosen to suit the types of aerosols to be detected. LIF lidars typically emit laser radiation in the ultraviolet region from 200 to 400 nm, as this wavelength range excites amino acids and other biomolecules present in the biological materials that produce fluorescence. The 266 and 355 nm are used to excite primarily the amino acid tryptophan and NADH respectively [5]. The advantage of detecting specific UV LIF information on biological molecules is limited to a modest range (a few kilometers) mainly because of the weak inelastic cross section of most fluorescing aerosols. Since this inelastic cross section is much lower than its elastic counter part for fluorescing aerosols, elastic lidar returns are more intense than the inelastic ones. Therefore, the combination of a long-range IR lidar to detect suspicious clouds and a short-range UV LIF lidar to discriminate biological aerosols is a highly promising approach to provide effective early warning [6]. The differential absorption lidar (DIAL) and scattering technique consists in evaluating the differential lidar backscatter attenuation between two laser beams having a slight shift in wavelength with one closely matched to the electronic transition of a targeted molecule. In this last technique, a Long-Wave Infrared (LWIR) Differential elastic Scattering (DISC) technology has proven to be promising to discriminate between biological simulants as well as interferents [7]. The main advantage of DISC over the UV LIF is an improved daytime sensitivity. Depolarisation ratio measurement using one or multiple wavelengths also appears to be promising [8].

Canada has adopted several measures to increase its readiness against the potential biological menace, one of which was the development of a lidar sensor for aerosol biological threat detection by Defence R&D Canada (DRDC) at the end of the 90's. This sensor, called SINBAHD (Stand-off Integrated Bioaerosol Active Hyperspectral Detection), is based on intensified range-gated spectrometric detection of laser-induced fluorescence (LIF). It demonstrated the capability of detecting and characterizing bioaerosols from a stand-off position using UV LIF [9]. In July 2007, SINBAHD participated to the international Suffield BioSense Trial 2007 (SBT07), a two-week trial held at DRDC- Suffield where different open-air wet releases of live and killed bioagent simulants and obscurants were performed. This paper intends to report on the SINBAHD participation and on the results obtained at that occasion.

2. TRIAL APPARATUS

The Canadian stand-off sensor SINBAHD and three different types of point sensors were deployed during the Suffield BioSense Trial 2007. The point sensors used for reference and correlation purposes were a low- and high-resolution slit samplers (LR, SSA), a Fluorescent Aerosol Particle Sensor (C-FLAPS) and an Aerodynamic Particle Sizer (APS). The slit samplers and C-FLAPS were used as point reference systems for all bacterial releases and the APS was used for all types of releases. Results from SINBAHD, the slit sampler and the APS will be presented herein.

2.1 Stand-off system: SINBAHD

SINBAHD is a completely self-sufficient lidar system, which includes the transmitter, receiver, electronics and cooling systems installed in a 12 m-long modified semi-trailer complemented with a diesel-powered generator . The sensor is schematized in Figure 1. The laser source is a UV Xenon-Fluoride excimer laser (GSI Lumonix, model PM-848) emitting around 150 mJ per pulse at 351 nm and a pulse repetition frequency (PRF) of 125 Hz. A visual channel, including a beam splitter (VBS), zoom lens and CCD optically inserted in the LIDAR emitter channel, allows the precise pointing of the laser beam at the target of interest. After passing through the 3.65x beam expander, the emitter divergence (FWHM, including pointing stability) is approximately 147 µrad (width) x 308 µrad (height). An adjustable 45-degree folding square mirror (FM) is placed at the center of the telescope-collecting aperture to obtain a co-axial LIDAR transmitter. A 50 cm by 33 cm elliptical steering mirror controlled by motorized gimbals is used to select the line of sight of the LIDAR. A 30 cm diameter Newtonian telescope (Space Optics Research Labs) of 127 cm focal length collects the returned radiation and focuses it at the entrance slit of the imaging spectrometer (Oriel, model MS260i). A beam splitter (SBS) followed by a 10-nm band pass filter centered at 350 nm (SF) and a photo-multiplier tube (PM), allow sampling of the elastic scattering. This photo-multiplier is connected to a transient recorder and provides elastic scatter returns as a function of range. This information is used to configure the width and position of the intensified range-gate. This elastic scattered radiation is blocked by two UV high-pass filters (FF) before entering the spectrometer. The 300 line/mm grating in combination with the 200 µm wide entrance slit of the spectrometer confer a spectral resolution of 4.8 nm and a span of 230 nm, optimized between 300 and 600 nm. An intensified CCD (ICCD) camera from Andor™ Technology detects the dispersed radiation at the exit window of the spectrometer. The 128×1024-pixels

CCD array is binned vertically and from the 1024 horizontal pixels, 675 are in the intensified region. The intensifier gate is synchronized with each fired laser pulse with a delay defining the range of the probed atmospheric cell. Between each laser pulse, the natural radiant contribution which is collected simultaneously with the fluorescence is sampled. The intensifier sensitivity combined with the 16-bit dynamic range of the camera and the spectral distribution of the collected signal over the CCD columns permit the detection of very low signal levels while retaining the spectral information.

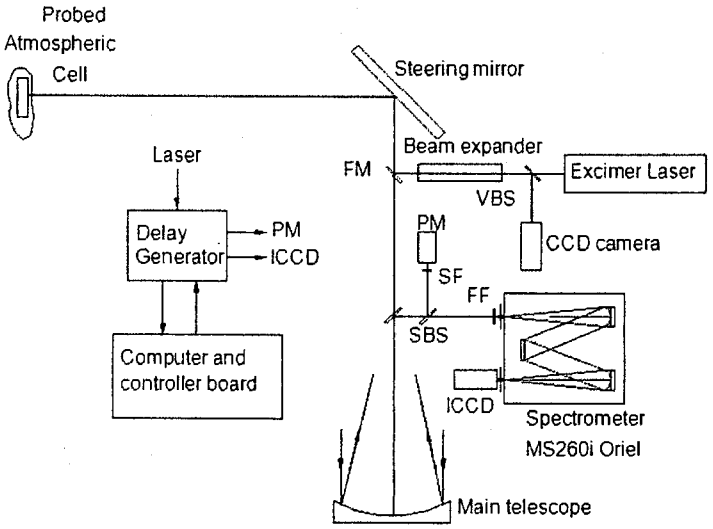

Fig. 1. Schematic representation of the Canadian standoff biological detection sensor: SINBAHD.

2.2 Slit samplers

The slit samplers draw ambient air through a slit orifice and onto a rotating plate containing growth media. After the plates are incubated, bacterial colonies are counted and bioaerosol concentration is calculated as a function of time based on the plate rotation speed and intake airflow. The resulting bioaerosol concentration is given in agent containing particles per litre of air (ACPLA). The low-resolution (LR) slit sampler (model STA 204, New Brunswick Scientific, Edison, NJ 08818-4005) had a rotation speed of 1 revolution/hr and was used to confirm bioaerosol cloud arrival on the grid, which is the physical location of the different reference sensors and target for the identified generated cloud. The high-resolution slit sampler array (SSA) consisted of 10 serially connected samplers (HF Research, custom-built), each with a rotation speed of 0.5 or 1 revolution/min providing a continuous 20 or 10-minutes effective collecting period, respectively. Any biological particles present in the aerosol impact the surface of the nutrient agar plate, and after an incubation period, live particles can be counted as bacterial colonies by a plate scanner (Synbiosis Ltd., Frederick, MD).

2.3 Aerodynamic Particle Sizer (APS)

An aerodynamic particle sizer (APS), model 3321 from TSI was used to evaluate the particle concentration in particle per litre of air (ppl) and in the mean time, extract the aerodynamic size profile of the probed particles. The APS sizes particles in the range from 0.5 to 20 micrometers using a sophisticated time-of-flight technique which measures aerodynamic diameter in real time. Because this latter parameter accounts for particle shape and is unaffected by the index of refraction or Mie scattering, it provides a better evaluation of the aerosol size distribution than other sensor based on light scattering like the C-FLAPS.

3. METHODOLOGY

Different bioaerosol simulants, growth media and interferents (Table 1) were released at the Colin Watson Aerosol Layout (CWAL) facility of Defence Research & Development Canada – Suffield during SBT07. This section details the main technical issues associated with the production of these releases and the trial methodology.

3.1 Simulant preparation

The two types of BG samples used during SBT07 were obtained from Dugway Proving Ground (DPG) and are identified as "old" and "new" BG. The old BG was produced in 1963 and has been used historically in the testing of biological detectors. It is a dry powder that contains approximately 5% fluidizer to prevent clumping. The New BG is a Danish BG produced in July 1996. It is also a dry powder containing approximately 5% fluidizer. Both BG samples are stored dry at -20 °C. For dissemination, BG samples were prepared as a 0.1% (w/v) solution in triple-distilled water. EH was grown in a nutrient broth fermentation system. Harvested material was unwashed. Batches averaged 2.3×10^9 colony forming unit per milliliter (cfu/ml). Nutrient Broth (NB) was prepared as 160 g in 20 litres of triple-distilled water before dissemination.

3.2 Dissemination

Simulant materials were placed in an agricultural sprayer (model AU8110, MicronAir) for dissemination. The sprayer contained a reservoir with mixing capability and was operated at approximately 1 liter per minute. It should be noted that the reservoir outlet was located at the bottom, ensuring that no material was left over after the dissemination. Each type of releases (live BG, live EH, and killed BG) used dedicated sprayers. Dissemination points was located at distances varying between 30 and 100 m from the point sensor grid in order to increase cloud concentration on the grid or simply to ensure that the cloud hit the grid under highly fluctuating wind conditions.

3.3 Trial methodology

The sprayer was mounted on a mobile platform circulating on the circumference of a circle centered on the CWAL grid (Figure 2). This platform was moved as a function of wind direction in order to position the aerosol cloud on the grid where the reference equipment was located (Figure 2). An overall of 58 crosswind releases were performed and slit samplers reference data were obtained for all bacterial releases. The reference equipment was located on an elevated platform about 2 meters above the ground; the C-FLAPS was slightly lower. The close proximity of these devices was important in order to generate good spatially correlated results. The LR was switched on manually by the trial operators 10 minutes before release start, while the SSA and C-FLAPS were switched-on remotely. The APS acquired data continuously during the entire trial period. SINBAHD was located at ranges of about 200, 470, and 990 meters, monitoring an atmospheric cell depth of 10 or 20 meters. Each acquisition was the result of 1000 integrated laser pulses and about 10 seconds were needed to perform the data acquisition cycle. For each release, SINBAHD data collection was initiated about 10 minutes before the release started and ended 10 minutes after the release had stopped.

TYPE	MATERIAL	INFORMATION
Bacteria spore	'Old' BG	*Bacillus atrophaeus (Bacillus subtilis* var. *niger* or *Bacillus globigii)*, powder, Batch 4, from Dugway Proving Ground (DPG).
	'New' BG	*Bacillus atrophaeus*, powder, origin from Denmark. Lot #19076-03267.
	killed BG	Old BG sample killed by either autoclaving or gamma-irradiation
Bacterial vegetative cells	EH	*Erwinia herbicola,* wet unwashed EH in the spent media (nutrient broth), from ATCC #33243.

Table. 1. Material released during Suffield BioSense Trial 2007.

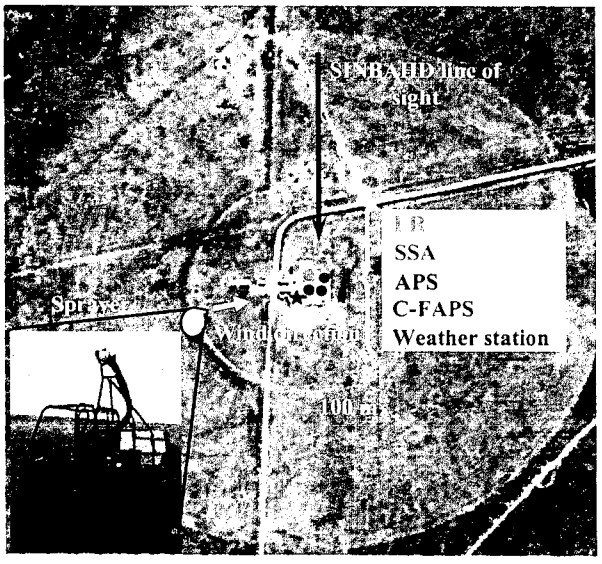

Fig. 2. Suffield BioSense Trial 2007 setup.

4. DATA PROCESSING

The sensitivity of SINBAHD was evaluated for different material during SBT07. For each release, a spectral signature was first extracted. A multivariate analysis [10] was then performed to extract the energetic contributions of the different released material based on their spectral signatures. This latter process was used to determine whether a specific material was detected, based on given detection limit criteria. Four times the standard deviation (4σ) of a given material energetic contribution while no cloud is present was used as the detection limit criteria. The energetic contribution was finally compared to the reference data from point sensors to evaluate the degree of correlation between SINBAHD and reference sensors and to obtain its sensitivity in the reference sensors ACPLA and ppl units.

4.1 Spectral signature extraction

The LIF emitted by the background aerosols and the different species studied were spectrally characterized. Every SINBAHD acquisition consisted of LIF collections from 1000 laser pulses emitted at 125 Hz in a selected window from which the ambient radiance, acquired between laser shot, was subtracted. The background LIF must be characterized since this fluorescent component is present in all acquisitions and must be included in the multivariate analysis. The background spectral signature was obtained by filtering and normalizing the spectral average of many background LIF acquisitions, from which the naturally occurring radiance signal was subtracted.

To extract the spectral signature of a specific released material, the first step is to subtract the naturally occurring fluorescence (obtained while the laser is not firing) from each LIF acquisition. The mean background LIF can then be calculated and subtracted from all other spectra considered to have a significant fluorescent signal originating from the released material. This step accounts for the background LIF while no specific material is present and for most of the intense Raman signals. A threshold comparison with the mean background integrated signal level is used to perform this step. The background LIF-subtracted signals are then averaged, smoothed, and normalized in energy over a predetermined spectral range to extract a representative LIF spectrum of the aerosol cloud being probed. Figure 3 presents 36 fluorescence acquisitions (red), their mean (green) and the calculated LIF spectral signature (black) obtained during a release of BG with a 20-m gate at a range of 200 m. Even though the signature presented in Figure 3extends from 400 to 597 nm, the energy normalization spectral range is limited to 425–597 nm. For the present study, the mean signature having the highest signal to noise ratio (SNR) from all the releases for a given material was used in the multivariate analysis to optimize the detection procedure. The SNR of a given signature is defined herein as the ratio of the signal amplitude mean over the standard deviation of all acquired signals within a given spectral bin.

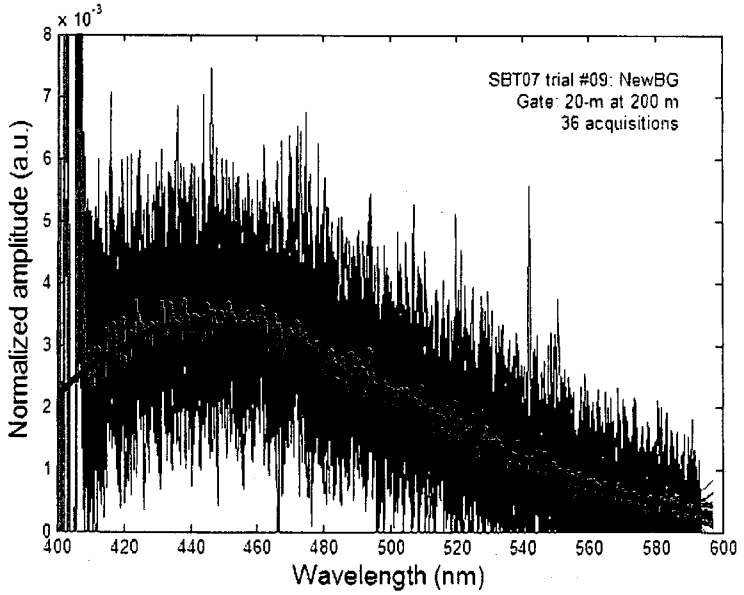

Fig. 3. Live New BG normalized signatures (black) obtained by SINBAHD with a 20-m gate at 200 m range; individual acquisitions in red, mean in green.

4.2 Multivariate analysis

A model [10] was developed based on the fluorescence lidar equation [11] for representing the signal acquired by a stand-off lidar sensor:

$$\frac{dE}{d\lambda}_{ba}(\lambda,\lambda_0,r) = n_{pu}E_0(\lambda_0)\cdot\xi(r)\frac{A_0}{r^2}\cdot t_{oe}(\lambda_0)\,t_{oc}(\lambda)\cdot t_{ae}(\lambda_0,r)\,t_{ac}(\lambda,\ r)\cdot\Delta r N_{ba}(r)\frac{d^2\sigma^F_{ba}}{d\,\Omega\,d\lambda}(\lambda_0,\lambda) \quad (1)$$

In equation (1), $dE/d\lambda_{ba}$ is the radiated energy per unit wavelength interval, collected at wavelength λ, from a single type of bioaerosol, *ba*, located at a range r, when excited by n_{pu} laser pulses, each of energy E_0, at a wavelength λ_0. ξ is the overlap function; A_0 is the aperture of the telescope; t_{oe} and t_{oc} are the overall spectral transmissions of the emitter and collector optics respectively; t_{ae} and t_{ac} are the atmospheric spectral transmissions over the emission and collection paths respectively; Δr is the depth of the atmospheric probed cell; N_{ba} is the averaged density of the bioaerosol *ba* in that cell. Finally, assuming isotropic fluorescence, the differential fluorescent cross-section of bioaerosol can be expressed as [10]:

$$\frac{d^2\sigma^F_{ba}}{d\Omega d\lambda}(\lambda_0,\lambda) = \frac{\Psi_{ba}(\lambda_0)\,A_{ba}}{4\pi}P_{ba}(\lambda_0,\lambda) \quad (2)$$

where $\Psi_{ba}(\lambda_0)$ is the effective quantum yield and A_{ba}, the effective projected area of the bioaerosol *ba*. P_{ba} is the spectral probability distribution of the inelastic induced photons which provides the classification capability. A multivariate analysis (MA) is used to process the collected data. The purpose of this data processing methodology is to separate signals associated with the different inelastic scatters: biofluorescence scatterer E_{is}, Raman scatters $E_{Raman\ line}$, or any other spectrally-distributed signals present in the collected spectra [10]. This technique represents the collected inelastic spectra E_λ as a linear combination of normalized spectral signatures $\vec{s}^{\,\lambda}_{is}$, which can be associated with known sources of inelastic scatters, *is*, and is expressed as follows:

$$\vec{E}_\lambda = E_{ba1}\vec{s}^{\,\lambda}_{ba1} + E_{ba2}\vec{s}^{\,\lambda}_{ba2} + \ldots + E_{N_2}\vec{s}^{\,\lambda}_{N_2} + E_{H_2O}\vec{s}^{\,\lambda}_{H_2O} + \ldots \quad \text{where} \sum_\lambda \left(\vec{s}^{\,\lambda}_{is}\right) = 1 \quad (3)$$

The bioaerosol spectral signatures, $\vec{s}^{\,\lambda}_{ba}$, which are sensor-dependent, can be obtained during well-controlled short-range releases of the bioaerosol of interest. The energetic contribution E_{is} extracted with the MA was performed using an algorithm implemented within the dedicated processing software called *SINBAHD virtual* [10].

4.3 Correlation evaluation

The correlation evaluation between the SINBAHD measured energetic contribution of a given material and reference equipments was performed numerically but judged, in many cases, not statistically valid due to the limited spatial correlation of the released cloud concentration sampled simultaneously by the different sensors. This is an important limitation of open-air releases refereed by multiple sensors. Consequently, a visual correlation assessment was performed and resulted in a more representative correlation evaluation. From this extracted correlation, SINBAHD sensitivity in ACPLA or ppl was derived. In most cases, the obtained detection limit represents an optimum evaluation since the releases were pure (except for the simultaneous dissemination of different aerosol types), the material signatures were known a priori and used in the MA, and the background was properly characterized.

5. RESULTS AND ANALYSIS

The normalized spectral signatures extracted from the data collected during Suffield BioSense Trial 2007 are presented in this section. The following interesting outcomes from these signatures results are initially discussed: signatures comparison between two different fermentation batches of *Bacillus atrophaeus* (5.1); difference and impact of a killing methodology on the signatures (5.2); signatures comparison between different growth batches of EH bacterial vegetative cells and bacterial BG spores (5.3); and EH signature robustness (5.4). SINBAHD MA results correlated with the reference point sensors are then presented (5.5). Using these correlated results, the detection limits in ACPLA and/or particles per liter of air (ppl) are evaluated. Finally the correlation between ppl and ACPLA data are evaluated (5.6).

5.1 Comparison between two different batches of *Bacillus atrophaeus*

Two different growth batches of *Bacillus atrophaeus* (BG) were tested: Old and New BG (Table 1). Figure 4 presents the spectral signatures obtained for all live BG material releases. From these results, it can be seen that the two batches of BG have similar spectral features. However, these apparently simple signatures come from a much more complex signal bundle (Fig.3) which would be characterized by a mean and a covariance matrix for the subsequent classification process. This indicates that the classification could eventually classify these two batches of BG in the same category and would not be able to discriminate between them. This latter classification output should be satisfactory in view of the detect-to-warn goal of stand-off biodetection systems.

5.2 Killed versus live BG material

The killed BG samples were disseminated in exactly the same way as their live counterparts and the corresponding fluorescence characteristics were compared. Figure 5 presents all the normalized spectral signatures of live (green) and either autoclaved (dark red) or gamma-irradiated (dashed light red) killed Old BG samples. These results show a slight discrepancy between the normalized spectral signatures of killed versus live BG material and no significant discrepancy between autoclaved versus gamma-irradiated Old BG material. However, considering the limited number of releases of the killed material and the fairly high variability of the different extracted signatures due to the intrinsic low SNR of BG material, it is difficult to evaluate the significance of these differences. Signatures with high SNR would enable a much valuable evaluation of the impact of the killing methodology on the material's spectral characteristics.

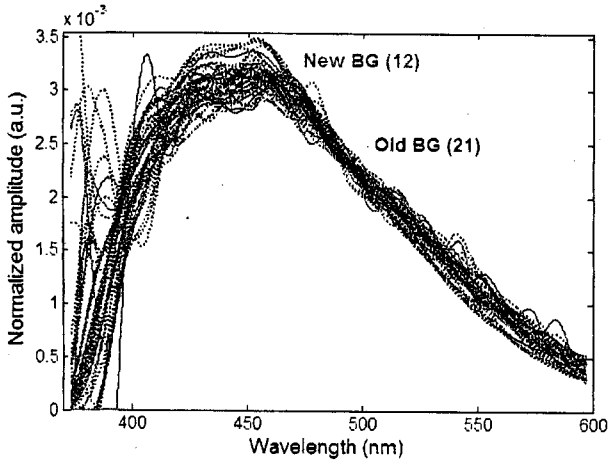

Fig. 4. New (green) and Old (red) normalized BG signatures obtained by SINBAHD with a 10 or 20-m gate at 200, 470 or 990-m range during SBT07.

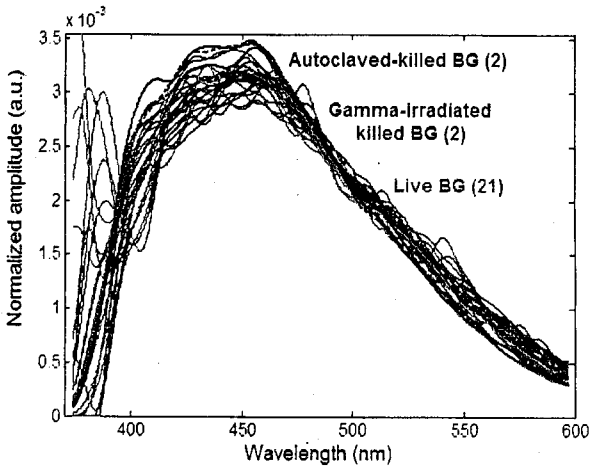

Fig. 5. Live (green) and either autoclaved (dark red) or gamma-irradiated killed (light red) Old BG signatures obtained by SINBAHD during SBT07.

5.3 Comparison between different EH growth batches and BG

The spectral signatures of different growth batches of bacterial vegetative EH cells are compared to the signatures of bacterial spores of *Bacillus atrophaeus* (BG) in Figure 6. The first observation is the significant discrepancies between the various EH signatures from different releases. The EH was grown at 27°C using a fermentation procedure in nutrient broth. To minimize variations, each batch followed the same procedure. These releases were performed at different periods over the two-week trial and at different ranges, and hence with different optical alignments. But in the past, these latter two variables did not show an impact on the acquired spectral signature [12]. Contamination during release is not a possible explanation since dedicated sprayers were used to disseminate EH material. In addition, each batch of EH was checked for purity prior to its use. Weaker discrepancies are also observed for signatures obtained from releases of the same EH growth batch on the same day: 2 releases of batch 12 on July 30th (light blue dashed curves) and 2 releases of batch 11 on July 31st (medium blue dashed curves). The observed variability of the spectral information obtained from EH releases were unexpected and raised some questions about signature robustness which will be revisited in the next

sub-section (5.4). The weather conditions could hardly explain the discrepancy since the signatures were collected within a two-week period during summer, under fairly stable weather conditions. The second observation from these results is that the two materials display spectral specificities. However, the variability of the extracted spectral characteristics of the EH tends to blur its specificity versus the BG signature. The rise in the EH fluorescence peak amplitude corresponds to a more pronounced negative spectral slope and a less extended spectra in the longer wavelength, when normalized over the 425 to 597 nm spectral range. It must be mentioned that EH comes in a liquid form and BG is a dry powder that is mixed with triple-distilled water before it is sprayed.

5.4 EH spectral signature robustness

The spectral characteristics of a given material may be influenced by parameters such as its origin, storage conditions, growth and preparation methods, state (wet or dry), dissemination process, or even the weather conditions during the dissemination. These variabilities enlarge the material signature sub-space within the multivariate space and can be problematic for a specific classification, since the different material subspaces will have a higher probably of overlapping. Various EH signatures from the 2005 JBSDS Demo II trial [12] and the JBSDS Increment II Tech Demo III trial in 2007 [13] were compared in order to assess this potential variability. Both of these acquisition campaigns took place at DPG, Utah, USA; in June 2005 and August 2007, respectively. The origins, viability in cfu/ml, state and dissemination methods were basically the same for all three trials. The only major dissimilarity would be the sample preparation methodology. Figure 7 compares the different spectral signatures obtained for different EH samples released during the three different trials. The two signatures obtained at DPG in 2005 (reddish lines) are consistent with each other but not with the ones obtained at DPG in 2007 (gold curves). Signatures obtained at Suffield 2007 (bluefish) either range in between the latter two subsets or extend farther down to the DPG 2007 side. The peak amplitude is found around 430 nm for DPG 2005 and Suffield 2007 but is around 438 nm for the signatures extracted from the DPG 2007 trial. The variability in the spectral signature of EH obtained from the Suffield 2007 trial appears less perplexing when they are compared with DPG 2005 and 2007 results. These observations tend to validate the hypothesis of variability due to the sample preparation methodology since all different releases consisted in the same ATCC EH material. It must be mentioned that the presented spectral signatures are not corrected for the instrument spectral response, meaning that no calibration process was performed on the data.

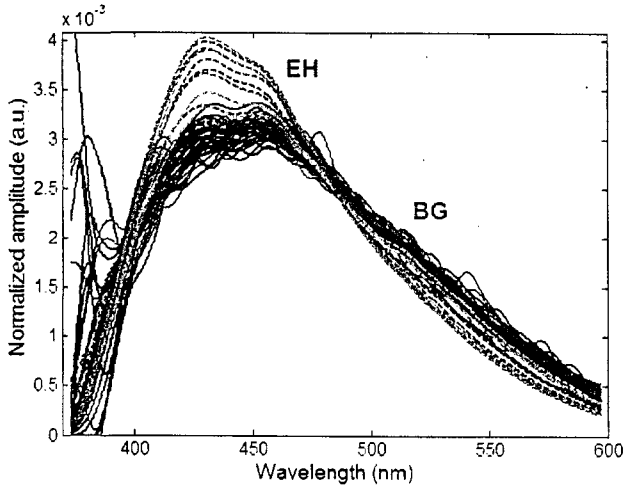

Fig. 6. Normalized fluorescence signatures of BG (green) and EH (bluish) obtained by SINBAHD during SBT07.

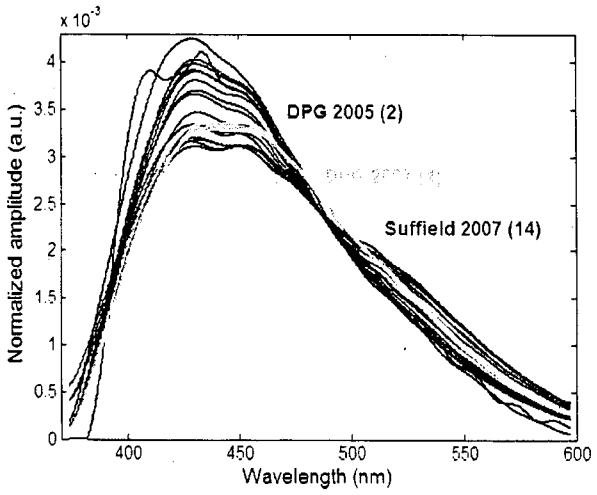

Fig. 7. Normalized spectral signatures for different EH samples obtained with SINBAHD at DPG in 2005 (red) and 2007 (gold) and at Suffield in 2007 (blue).

5.5 Multivariate analysis and correlation between standoff and point sensors

The multivariate analysis gives the amplitude of a given normalized signature within the linear combination (Equation 3), which represents the estimated energetic contribution of the bioaerosol based on a least-squares best fit. These later

energetic contributions are then visually correlated with the reference sensors output. Figure 8 presents SINBAHD MA results (pink dashed line) and the APS data (blue line) for the live Old BG release (#T48). The visually obtained correlation is quite good both in time and in amplitude. The APS probes all the particles present in the air whether or not they show fluorescence. This can be seen in the up-rising background level after the release (00:57). The APS sensor is very useful since the output data can be seen in real time versus several hours or days for the slit samplers. However the data reliability for fluorescence correlation purposes is highly dependant on the stability in concentration (ppl) of the background aerosols. This latter aspect would be much less critical if the releases were performed in an aerosol chamber, in which case the background aerosols would be better controlled, and thus more stable in time compared to open-air releases. The visually assessed correlation allows extracting SINBAHD sensitivity in ppl, corresponding to the 4σ level. For this particular release, the extracted detection limit for a 20-m cloud of Old BG at 990 m is about 290 ppl above the background-level concentration. The calculated detection limit has a high uncertainty mainly due to the data processing. Indeed, depending on the different signatures used in the MA, the energetic contributions may differ and no evaluation of this variability was done under the present study.

Figure 9 presents SINBAHD MA results (pink dashed line) and the slit sampler data (blue line) for the same T48 release. The obtained correlation is once again quite good both in time and in amplitude. The slit samplers probed only during the 10 minutes of the release. But since the cloud takes some time to reach the grid, some background data is also included in the slit sampler data, which is needed to perform the correlation between the two sensors. From this visual correlation evaluation, the obtained detection limit is around 50 ACPLA for a 20-m cloud of Old BG at 990 m.

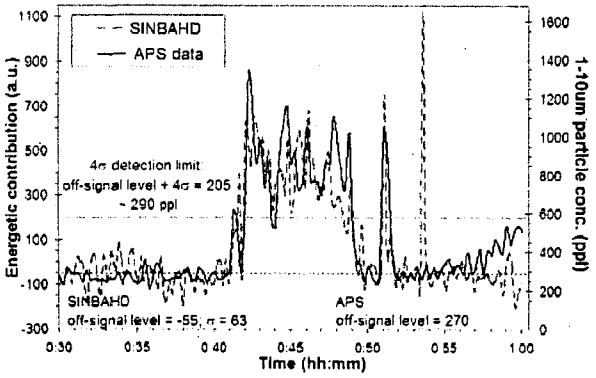

Fig. 8. SINBAHD multivariate analysis results: amplitude of live Old BG (dashed pink) and APS data (solid blue line) for T48 live Old BG (20-m gate width at 990 m).

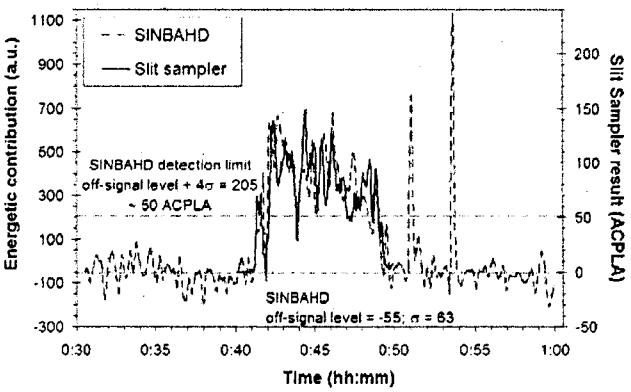

Fig. 9. SINBAHD multivariate analysis results: amplitude of live Old BG (dashed pink) and slit sampler data (solid blue line) for T48 live Old BG (20-m gate width at 990 m).

A gate/range normalization process based on the model presented in section 4.2 (Equation 1) can be applied in order to compare the different extracted detection limits. Additionally, the assumption that the SINBAHD output metric follows a Poisson noise distribution (shot noise) is made. This latter hypothesis is not rigorous but is a good approximation even for very small signal. Assuming Poisson statistics, the standard deviation of the output signal is the square root of the mean signal as well as the SNR. The gate/range normalization process applied on the extracted detection limit includes the dependency on the gate width Δr and range r, as modeled in equation 4. The signal is thus not corrected for the other parameters influencing the measured signal, such as the emitted laser energy, the atmospheric transmission or the transmitter alignment, which are approximated as constant.

$$Limit_{norm}(\Delta r_o, r_o) = Limit(\Delta r, r) \cdot \sqrt{\frac{\Delta r / r^2}{\Delta r_o / r_o^2}} \qquad (4)$$

Figure 10 presents graphically all detection limits with a gate/range normalized for a detection limit based on a 10-m long cloud located at 1 km derived from the visual correlation assessment processed with BG releases. The inconsistent result from release #52 (Fig.10) could be explained by the high noise level in the SINBAHD output, which is probably due the higher ambient signal present at 20:30 compared to night-time releases. The calculated BG detection limit

appears to be dependant on the range (the gate width was fairly constant over the trial period) at which the acquisition was performed (Fig. 10). As mentioned previously, the Poisson noise distribution used to perform the extrapolation to a given range is simple but not rigorous, which is probably the main explanation for the observed range dependency. On the model side, the atmospheric transmission and the overlap function could also induce a dependency in range. The former is expected to increase slightly with shorter range while the overlap function, which depends on the transmitter alignment, is updated each time the system-to-grid range is modified. The results from BG releases performed at 990 m yield detection limits around 35-80 ACPLA for a 10-m cloud at 1 km.

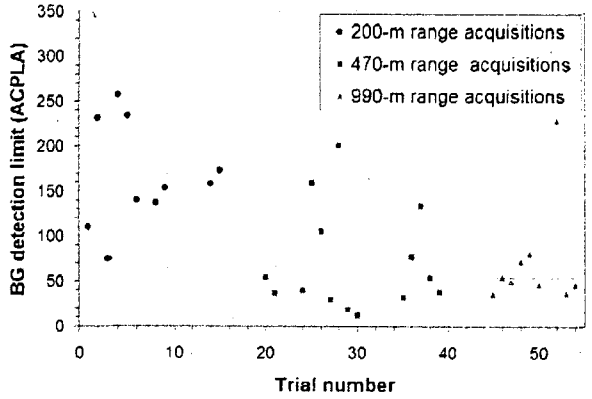

Fig. 10. SINBAHD detection limit normalized for a 10-m BG cloud at 1 km extrapolated from releases performed at 200 m (blue circle), 470 m (pink square) and 990 m (green triangle) range.

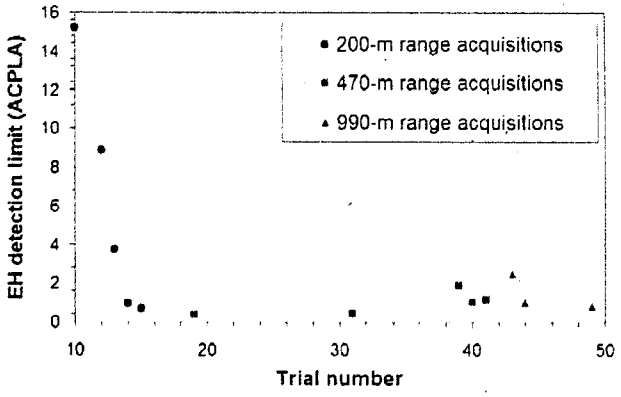

Fig. 11. SINBAHD detection limit normalized for a 10-m EH cloud located at 1 km extrapolated from releases performed at 200 m (blue circle), 470 m (pink square) and 990 m (green triangle) range.

Figure 11 presents the corresponding results for EH releases where detection limits are extrapolated for a 10-m thick cloud located at 1 km. In this case, with the exception of the first three results obtained at 200 m, all extrapolated detection limits are of the same magnitude even though trials were performed with the same trial configurations than the BG releases shown in Fig.10. Indeed, 10 out of 13 extracted detection limits are between 0.4 and 2.7 ACPLA and the other three are a few times higher but still within the same order of magnitude. The main difference between the BG and EH signals acquired by SINBAHD is their relative fluorescence intensity, which could be at the origin of the variability of the relation linking the normalized detection limit as a function of the ranges of the measurements. Indeed, when looking at the SNR of the SINBAHD output (i.e. the BG energetic contribution obtained from the multivariate analysis), it appears that the SNR does not improve as much as the model states with shorter distances. This observation is quite valuable and additional theoretical development, especially noise considerations, will be needed to better model the sensitivity of such LIDAR instrument as a function of range.

5.6 The correlation between ppl and ACPLA data

The evaluation of the correlation between the APS and the slit samplers data was performed for each release data set. The results are presented in Figure 12 in terms of the averaged ratios of the ACPLA reading versus particle concentration integrated between 1 to 10 μm (ppl) (ACPLA/ppl × 100). Figure 12 presents the extracted values from the visual correlation assessment for Old BG (light green diamonds)), new BG (dark green triangles) and EH (blue squares) releases. No significant discrepancy was observed for the ACPLA-ppl ratio between the Old and the New BG releases. This ACPLA-ppl ratio ranged from 2 to 29% and from 1 to 6% and had a mean value of 12% and 3% for BG and EH releases, respectively.

The obtained correlation between the ACPLA and ppl data are specific to the sprayer used to perform the dissemination and also probably on the environmental conditions from which these correlation were derived. Indeed, the ACPLA output readings are highly influenced by the clumping and the agglomeration of particles since this unit counts the number of particles that contain viable agent regardless of the number of agents present in that particle. For example, an average liter of air containing 100 particles each containing only one agent will give a reading of 100 ACPLA compared to a reading of 10 ACPLA for only 10 particles, each containing 10 agents. This means that the same slurry bacterial

mixture will produce higher ACPLA readings under aerosolizing conditions that minimize particle size and clumping. This implies that the ACPLA-ppl ratio will most likely vary with the type of sprayer used to perform the dissemination or, to a certain extent, the environmental conditions. It must be considered that the derived ACPLA-ppl ratios were obtained from open-air releases during which spatial and temporal correlation of the two point sensors was limited due primarily to the non-homogeneity of the disseminated cloud. This latter aspect may explain, in part, the significant variability of the derived ACPLA-ppl ratios (Fig. 12).

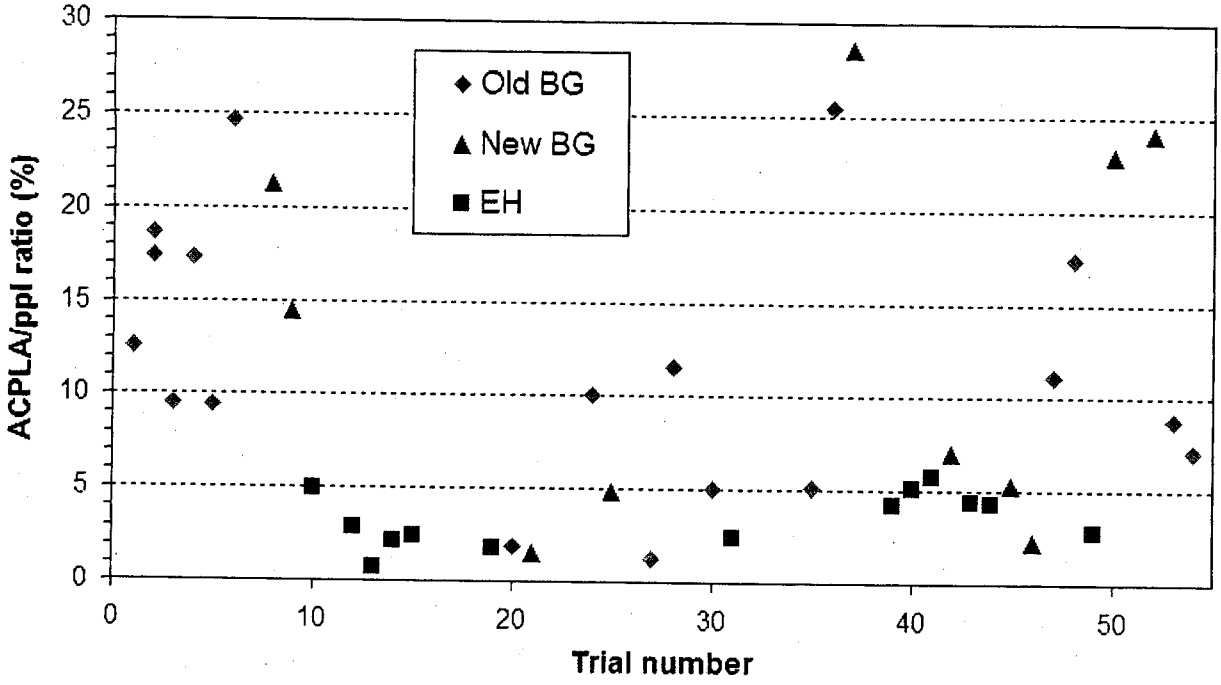

Fig. 12. ACPLA to ppl ratios derived from visual correlation of all Old BG (light green diamonds), New BG (dark green triangles) and EH (blue squares) releases performed during SBT07.

6. CONCLUSION

During Suffield BioSense Trial 2007, SINBAHD measured the spectral characteristics of: two different growth batches of *Bacillus atrophaeus* spores (BG); gamma-irradiated killed versus autoclaved killed BG; killed versus live bacterial spores samples of BG, 12 different batches of the bacterial vegetative cell *Erwinia herbicola* (EH) during cross-wind open-air releases. The two different batches of BG (Old and New) did not show significant differences in their respective signatures. The normalized signatures of the gamma-irradiated and autoclave-killed Old BG samples did not show significant differences but slight discrepancies were observed between killed and live old BG samples. These latter observations imply that the killing methodology affects only slightly the spectral signature of the material in the case of BG bacterial spores. However, the spectral signatures of different batches of EH showed significant variability. This last result provides instructive insights on the limits of the signature robustness, which is suspected to be related to the variations in the material preparation methodology.

A multivariate analysis (MA) was performed on SINBAHD acquired data to extract the bioaerosol energetic contributions based on least-squares best fit analyses. A correlation assessment was performed between these energetic contributions and referee point sensors outputs, allowing the evaluation of the 4σ sensitivity for a given aerosol cloud depth and range. The sensitivity derived from releases performed at 990 m and normalized for a 10-m cloud of BG and EH at 1 km indicates detection limits around 36-80 and a few ACPLA, respectively. Finally, correlation between ACPLA and ppl sensors data has given ratios ranging from 2 to 29% with a mean value of 12% for BG and ratios from 1 to 6% with a mean of 3% for EH. It must be noted that these correlations were derived from open-air releases which are not optimally correlated spatially. Nevertheless, these results clearly show a correlation between the APS and the slit sampler sensor readings. These observed correlations open new possibilities to referencing biological aerosol cloud in

ppl and estimates the concentration of the cloud in ACPLA based on the type of produced bioaerosols and the method of dissemination. The simpler ppl approach may be useful when the aerosol cloud concentration is too high to be characterized with classical slit samplers, when precise ACPLA referencing is not required or simply when the specific laboratory apparatus are not available. .

7. ACKNOWLEDGMENTS

SINBAHD has been made possible with funding originating from the Technological Investment Funds (TIF-16qd13), a Defence Research and Development Canada (DRDC) program initiated to support scientific investigation of high risk concepts but with strong potential for the Canadian defence communities. SINBAHD participation to the Suffield 2007 trial was made possible with funding originating from the BioSense Technology Demonstration Project . Furthermore, the data acquisition campaign for this article would not have been possible without the valuable trial participation of Denis Nadeau and Laurie Stadnyk.

REFERENCES

[1] Kortepeter, M.G. and Parker, G.W., "Potential Biological Weapons Threats", Emerging Infectious Diseases, 5(4), 523-527 (1999).

[2] National Research Council, [Sensor systems for biological agent attacks], the national academies press, Washington, D.C., chap. 4 (2005).

[3] Condatore, Jr., L. A., Guthrie, R. B., Bradshaw, B. J., Logan, K. E., Lingvay, L. S., Smith, T. H., Kaffenberger, T. S., Jezek, B. W., Cannaliato, V. J., Ginley, W. J. and Hungate, W. S., "U.S. Army Soldier and Biological Chemical Command Counterproliferatioin Long-Range Biological Standoff Detection System," Proc.SPIE 3707, 188-196 (1999).

[4] Gelbwachs, J. and Birnbaum, M., "Fluorescence of Atmospheric Aerosols and Lidar Implications," Applied Optics, 12(10), 2442 (1973).

[5] Hill, S.C., Pinnick, R.G., Niles, S., Pan, Y.L., Holler, S., Chang, R.K., Bottiger, J., Chen, B.T., Orr, C.S. and Feather, G., "Real-time measurement of fluorescence spectra from single airborne biological particles," Field Analytical Chemistry and Technology, **3**, 221-239 (1999).

[6] Buteau, S., Lahaie, P., Rowsell, S., Rustad, G., Baxter, K., Castle, M., Foot, V., Vanderbeek, R. and Warren, R., "Final Report for Task Group (RTG-55) on Laser based stand-off detection of biological agents," NATO RTO SET098 TG55 final report, 76pp. (2008).

[7] Warren, R. E. and Vanderbeek, R., "Estimation of multiple-aerosol concentration and backscatter using multi-wavelength range-resolved lidar," Proc. SPIE 6756, 67560D (2007).

[8] Lee, H. S., Hwang, I.H., Lee, S., Li, G., Serino, R.M. and Prasad, C.R., "Depolarisation for enhancing standoff lidar bio-aerosol discrimination," Proc. of the 7th Joint Conference on Standoff detection for chemical and biological defence, Williamsburg, (2006).

[9] Simard, J.R., Roy, G., Mathieu, P., Larochelle, V., McFee, J. and Ho, J., "Standoff sensing of bioaerosols using intensified range-gated spectral analysis of laser-induced fluorescence," IEEE Trans. on Geoscience and Remote Sensing, 42(4), 865-874 (2004).

[10] Simard, J.-R., Roy, G., Mathieu, P., Larochelle, V., McFee, J. E. and Ho, J., "Standoff Integrated Bioaerosol Active Hyperspectral Detection (SINBAHD): Final report, " DREV TR 2002-125, 118 pp. (2003).

[11] Measures, R. M., [Laser Remote Sensing: Fundamentals and Applications], John Wiley & Sons, Inc., Chap. 7.4 (1984).

[12] Buteau, S., Simard, J.-R., Déry, B., Roy, G., Lahaie, P., Mathieu, P., Ho, J. and McFee, J., "Bioaerosols Laser-Induced Fluorescence provides specific robust signatures for standoff detection", Proc.SPIE 6378, 637813 (2006).

[13] Buteau, S. and Simard, J.-R., "Bioaerosols standoff detection of spectrally resolved laser-induced fluorescence," Proc. of Chemical and Biological defense 2008 - physical science and technology conference, New Orleans, USA, (2008).